Thermally Induced Synchronous Vibration Instability in a Magnetic Bearing Supported High-speed Rotor

Naohiko Takahashi, Haruo Miura
Tsuchiura Research Laboratory
Hitachi Plant Technologies, Ltd.
603 Kandatsu-machi, Tsuchiura, 300-0013, Japan
naohiko.takahashi.qb@hitachi-pt.com
hauo.miura.wm@hitachi-pt.com

Yasuo Fukushima
Tsuchiura Works
Hitachi Plant Technologies, Ltd.
603 Kandatsu-machi, Tsuchiura, 300-0013, Japan
yauo.fukushima.hj@hitachi-pt.com

***Abstract* – This paper describes a synchronous vibration instability problem that occurred on a two-stage overhung centrifugal compressor. The authors encountered an unbalance vibration that increased spirally in a polar plot at/near the first bending critical speed. An iron loss concentration and a thermal bend by heat have been identified as the cause of the phenomenon, because the vibration stops increasing, when an unbalance force rejection control (UFRC) is applied. In order to exceed the first bending critical speed stably, an rotor unbalance measurement under UFRC and a rapid speed acceleration/deceleration are carried out. The vibration behaviours around the critical speed are simulated and verified experimentally. The stability limit that is depending on rotational speed is calculated and the most important parameter $|H/P|$ in the calculation are determined by measurements.**

***Index Terms* – Unstable Vibration, Iron Losses, Thermal Bend, Unbalance Force, Spiral Vibration**

I. Introduction

For active magnetic bearings (AMB), some types of loss such as windage loss on the bearing gap, copper loss on the coil, and iron loss on the iron core are caused. Among them, iron loss occurs both on the stator portion and rotating portion. As a problem caused by heat generation in the bearing, Ishida et al. reported the observation of rotor thermal bending in a high-speed motor with AMB [1]. Concerning the thermal bending of the rotor, we also experienced a symptom of vibration increase that was caused by thermal deformation of the rotor in an experimental machine with a flexible rotor [2]. Since greater iron loss occurs at a spot where magnetic flux density is greater, if magnetic flux density is concentrated on a spot of the bearing rotor due to an unbalance vibration control, the distribution of iron loss is also subject to bias. This is the cause of thermal bending. The thermal bending creates a new unbalance forces, and this generates a more flux concentration on the rotor. The vibration increase is caused by this vicious cycle.

For the vibrations induced by thermal bending of the rotor, the vibration induced by contact between the stator and rotor (rubbing), and the vibration induced by the unevenness of the temperature of the oil film on an oil bearing (Morton effect) are heretofore known [3]-[5]. The thermally induced vibration on AMB has a similar mechanism to these vibrations.

As mentioned in [2], we were not able to avoid the thermally induced vibration as a result. After that, we experienced a similar vibration symptom at the critical speed in the first bending mode of a high-speed turbo compressor. In this study, we have actually passed this critical speed, and verified the behaviour of the thermally induced vibration below/beyond the critical speed. To pass the critical speed, first of all, we minimized the unbalance vibration by a balance correction method not influenced by thermal bending. Next, we minimized the heat applied to the rotor and prevent the vibration increase by shortening the time of using the unbalance vibration control (N-ps control [6]). By these methods, we have made it possible to pass the critical speed against the thermal bending, and confirm the vibration behaviour [2] expected below/beyond the critical speed by actual measurement. In addition, we have presented a simple model to evaluate the stability of thermally induced vibration, and shown the dependency of the stability on the rotational speed. We have actually measured the parameter, $|H/P|$, which influences this stability, and compared the values with calculated values.

II. High-speed Turbo Compressor

A. Compressor Overall Structure

Fig. 1 shows the outline diagram of the high-speed turbo compressor that thermally induces vibration of the rotor similar to the vibration mentioned in [2]. The rotor is placed horizontally, and the motor at the centre of the rotor is a permanent-magnetic DC brushless motor with a rated speed of 55000 min^{-1}. The rotor is supported by AMBs placed outside the motor core. Two internal propellers are fixed to the rotor with overhanging outside the bearings. The total mass of the rotor is approximately 24 kg. Heat generation in the motor and bearings is reduced by cooled air blown into the clearance between the rotor and stator and between the rotor and bearings, and by cooled water flowing through the jacket covering the motor stator.

B. Magnetic Bearing System

The radial bearing is a hetero-polar type with an internal diameter of 64 mm. The thrust bearing is a C-shape type with a disk diameter of 125 mm. The design load of the bearing is 734 N for the radial bearings and 2740 N for the thrust bearing. The power amplifier driving the bearing coil is a PWM type with a maximum current of 15 A and a supply voltage of 300 V, and its driving method is class A. The displacement sensors for detecting rotor displacement are placed adjacently to the radial bearings. The controller consists of a DSP board (TI DSP: TMS320C6713). The sampling frequency is 20 kHz.

C. Rotor Vibration Modes

Fig. 2 shows the shape of the vibration mode of the rotor, calculated while assuming that the bearing supports are in a free-free condition. The vibration mode shapes are almost symmetric. Since only one displacement sensor is equipped on the right and left sides respectively, the vibration mode shape recognized by the sensors is either in the parallel mode or conical mode. The first bending mode is classified into the parallel system, and the second mode the conical system. The natural frequency is 611.7 Hz for the first bending mode and 1241 Hz for the second bending mode. Therefore, the rated speed, 55000 min^{-1}, is located between the first bending critical speed and second bending critical speed.

III. Bearing Control System

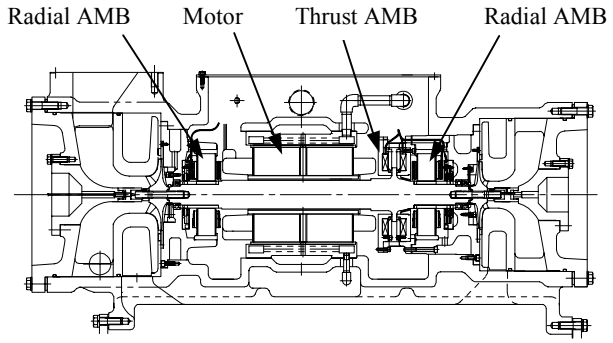

Fig. 1 High-speed turbo compressor

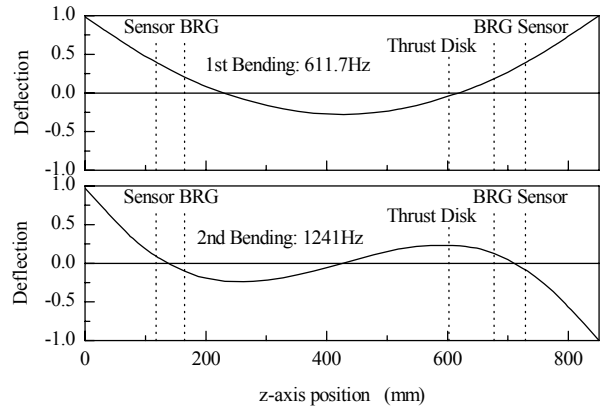

Fig. 2 Free-free mode shapes

A. Control System Configuration

For the control system of the radial bearing, the vibration modes of the rotor are classified into the parallel system and conical system, and a mode controller is assigned to each system by the mode control. The x and y axes are defined as the coordinates indicating the positions of the rotor in the directions of the diameter. The x and y axes are at right angles to each other and they are at an angle of 45° in the vertical direction. The anisotropy of the mechanical structure in the x/y-axes directions is negligible. By the displacement sensors placed on the right and left ends respectively, x_1/y_1 and x_2/y_2 can be measured, respectively, as displacement in the x/y-axes directions. Fig. 3 shows a schematic of the control system of the x-axis. The control system of the y-axis is the same control system as applied to the x-axis. The controller is configured with the parallel mode controller, conical mode controller, and tracking filter. For displacement signals x_1 and x_2, the manipulated variable output from the controller (command signals to the power amplifier), c_{x1} and c_{x2}, are calculated as follows:

$$\begin{bmatrix} x_p \\ x_c \end{bmatrix} = \begin{bmatrix} u_{11} & u_{12} \\ u_{21} & u_{22} \end{bmatrix} \begin{bmatrix} x_1 \\ x_2 \end{bmatrix} \tag{1}$$

$$\begin{bmatrix} c_{xp} \\ c_{xc} \end{bmatrix} = \begin{bmatrix} -G_{cc} & 0 \\ 0 & -G_{cp} \end{bmatrix} \begin{bmatrix} x_p \\ x_c \end{bmatrix} \tag{2}$$

$$\begin{bmatrix} c_{x1} \\ c_{x2} \end{bmatrix} = \begin{bmatrix} v_{11} & v_{12} \\ v_{21} & v_{22} \end{bmatrix} \begin{bmatrix} c_{xp} \\ c_{xc} \end{bmatrix}. \tag{3}$$

Here, there are the following relations:

$$G_{cp} = C_p(1 - G_n) - k_{nps} G_{nps},$$
$$G_{cp} = C_c(1 - G_n).$$

C_p, C_c, G_n, and G_{nps} are the transfer functions of the parallel mode controller, conical mode controller, tracking filter, and phase-shifting tracking filter, respectively. k_{nps} is the feedback gain of the unbalance vibration control by the phase-shifting tracking filter. u_{ij} and v_{ij} (i, j = 1, 2) are the operation parameters for mode separation and mode synthesis, respectively. Suffixes 1 and 2 mean the first stage (left side of Fig. 1) and the second stage (right side of Fig. 1), respectively. x_p and x_c are the mode displacements

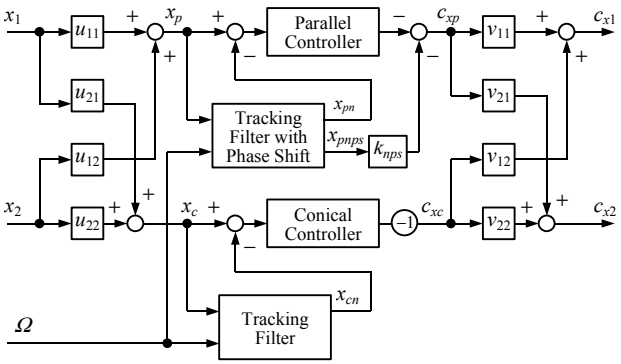

Fig.3 Block diagram of control system

of the parallel mode and conical mode, respectively, and c_{xp} and c_{xc} are the manipulated variables of the parallel mode control and conical mode control.

The parallel/conical mode controllers, C_p and C_c, are configured with a phase lead circuit, an integration circuit, and three second-order filters connected in series. The tracking filter, G_n, is a filter to extract only the frequency component equivalent to the rotational speed as following the rotational speed. Moreover, the tracking filter with a phase shifting function, G_{nps}, can shift the phase between the input and output signals arbitrarily.

B. Unbalance Vibration Control

In order to achieve the rated speed, it is necessary to pass the critical speeds of the two rigid modes and first bending mode, and the unbalance vibration control is the most serious problem in the first bending mode among the critical speeds. The control performance for unbalance vibration is determined by the gains and phases of the controller at rotational frequencies. The transfer functions of the tracking filter and phase-shifting tracking filter have the following relations to the rotational speed, Ω:

$$\begin{aligned} G_n(j\Omega) &= 1, \\ G_{nps}(j\Omega) &= e^{j\alpha}, \end{aligned} \tag{4}$$

where, j is imaginary unit $\sqrt{-1}$, α is the variable of phase shifting, which can be set arbitrarily. When these filters are operating, (2) is expressed as follows:

$$\begin{bmatrix} c_{xp} \\ c_{xc} \end{bmatrix} = \begin{bmatrix} -k_{nps}e^{j\alpha} & 0 \\ 0 & 0 \end{bmatrix} \begin{bmatrix} x_p \\ x_c \end{bmatrix}. \tag{5}$$

The feedback control of gain k_{nps} and phase α is operative for the unbalance vibration of the first bending mode. In this paper, this control is called the N-ps control. As shown in Fig. 3, this control, N-ps, is operative only for the parallel system. As for the component of (5), the feedback gain of the conical system is zero. This is called unbalance force rejection control (UFRC), which is a method to eliminate the control force for unbalance vibration. In the conical system, UFRC is applied in the range where rotational speed exceeds the critical speed of the rigid mode.

IV. Mechanism of Thermally Induced Vibration

A. Chain of magnetic force, iron loss, and thermal deformation

AMB suppresses the unbalance vibration caused in the rotor by the magnetic attractive force. This force is determined by the amount of the magnetic flux penetrating the air gap. The magnetic attractive force increases with the magnetic flux density. On the other hand, the iron core on the rotor side of the AMB (ordinarily a magnetic steel sheet) is exposed to the alternation of magnetic flux by its rotation, so that iron loss (eddy current loss and hysteresis loss) is caused. This iron loss increases as the magnetic flux density increases.

Now, we assume that the rotational speed is lower than the critical speed, and the relation between an unbalance force f_u and a rotational displacement r is as shown in Fig. 4. Here, the AMB system detects the rotor displacement r, and generates a magnetic attractive force f_b. At the spot exerted by the magnetic attractive force f_b, a magnetic flux density increases and an iron loss occurs together. Since unbalance force causes this iron loss, the iron loss concentration is located at a specific position in the view from the rotor. Consequently, when the AMB system attempts to control unbalance vibration, a static temperature gradient due to the concentration of iron loss occurs on the iron core of the rotor, so that thermal deformation is induced. When the iron core is thermally deformed, a thermal deformation, as shown in Fig. 5, occurs over the entire rotor, so that a new unbalance force is induced. If such a chain circulates due to the unbalance vibration control, the unbalance vibration increases at worst case.

B. Modeling for Stability Evaluation

Since the deformation speed of the rotor when thermally induced vibration occurs is much slower than the rotational speed, the amplitude and phase of the unbalance vibration

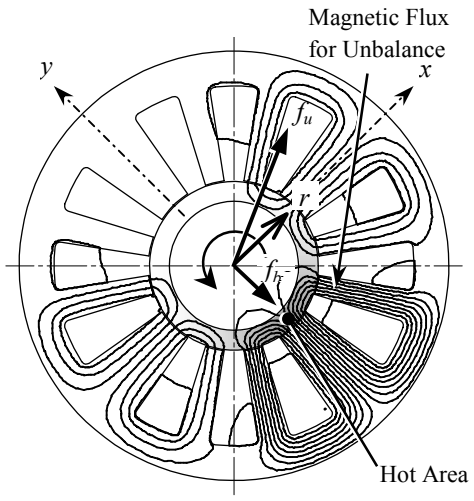

Fig. 4 Hot area due to magnetic flux

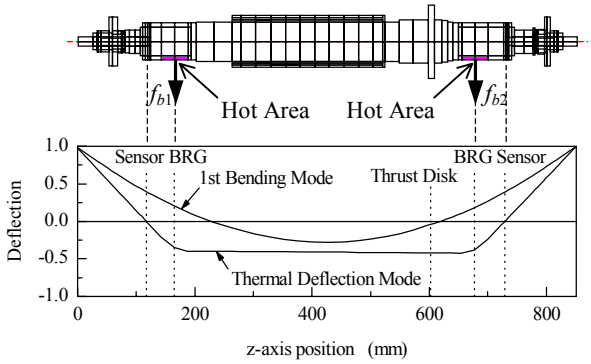

Fig.5 Thermal deformation mode and 1st bending mode

induced by thermal deformation are in the quasi-steady-state. Hence, the behavior of thermally induced vibration can be analyzed by modeling the static characteristic of the rotational speed component of the AMB rotor system.

This time, thermally induced vibration was problematic in the first bending vibration mode. Hence, to facilitate analysis, only the parallel system is considered and the conical system is ignored in the control system of Fig. 3. In addition, no anisotropy is assumed in the x and y axes directions, and an expression using complex number is introduced [7]. It is assumed that $f_u e^{j\Omega t}$ acts on the parallel system as initial unbalance. f_u is an complex number indicating the magnitude and phase of initial unbalance force. In the same way, expressing the unbalance vibration component of the parallel mode displacement as r, and the unbalance control component of the manipulated variable output by the parallel mode controller as f_b using complex numbers, a model with two inputs and one output like the following equations can be formulated:

$$r = \left(P + \frac{H}{\tau s + 1} \right) f_b + W f_u \tag{6}$$

$$f_b = -Cr \tag{7}$$

$$P = -\frac{P_0(\omega_z{}^2 - \Omega^2)}{(\omega_0{}^2 + \Omega^2)(\omega_n{}^2 - \Omega^2)} \tag{8}$$

$$H = -\frac{H_0}{(\omega_0{}^2 + \Omega^2)(\omega_n{}^2 - \Omega^2)} \tag{9}$$

where, W is a compliance of the rotor to the initial unbalance force f_u, and C is the transfer characteristic of the parallel mode controller at a rotation frequency. P is the compliance of the rotor, and up to the angular frequency of first bending critical speed ω_n is included in the equation. ω_z indicates the angular frequency of zero in the parallel system, and ω_0 indicates an unstable pole generated by a negative spring in the AMB. P_0 is a parameter depending on the mass and the mode shape of the rotor, which is a real number. The actual values obtained from the frequency responses of the rotor by an excitation test were ω_n = 3782 rad/s, ω_z = 2689 rad/s, and ω_0 = 155 rad/s. H is a compliance related to the thermally induced unbalance, and τ is the time constant of the thermal deformation. The model equation of H is determined based on the calculated frequency response by applying unbalance forces. The unbalance forces are determined by decentering the shaft centerline along the thermal deformation line in Fig. 5. H does not have a zero unlike in the case of P. The reason is as follows: The unbalance forces caused by thermal deformation shows an opposite-phase between the overhanging portion and the rotor center, so that the vibration mode does not have any zero displacement at the sensor between the frequency range in which the rigid mode is conspicuous and the frequency range in which the first bending mode is conspicuous. H_0 is a real number used to indicate the ease of thermal deformation. In order to obtain this value, calculations or experiments on thermal deformation are necessary.

The relation between (6) and (7) is illustrated as a block diagram shown in Fig. 6. This diagram indicates that the manipulated variable by the controller influences thermal dynamics as well, and this influence is circulated by feedback control.

Since $\alpha = \pi/2$ is set in the N-ps control for the first bending mode, a phase leading feedback of 90° is to be applied. This is equivalent to replace C in (7) with jk_{nps}. Now, the condition for keeping thermally induced vibration stable is as follows:

$$-H < P + \frac{1}{k_{nps}{}^2 P} \tag{10}$$

Since $P = \infty$ and $H = \infty$ at the first bending critical speed ($\Omega = \omega_n$), the above inequation becomes:

$$-\frac{H}{P} < 1 . \tag{11}$$

If the above condition is satisfied, the thermally induced vibration becomes stable regardless of control system.

The time responses of the displacement vector calculated from (6), (7), (8), and (9) are as shown in Fig. 7. Fig. 7(a) shows a case whereby the rotational speed is below the critical speed, and Fig. 7(b) shows the opposite case. In these calculation, $|H/P|$ was assumed as 1.55 at $\Omega = \omega_n$. The results of this calculation show that the variation of the displacement vector (spiral direction) differs depending on whether the rotational speed is below or

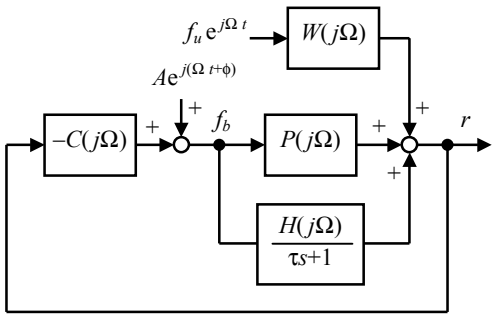

Fig.6 Model for thermally induced synchronous vibration

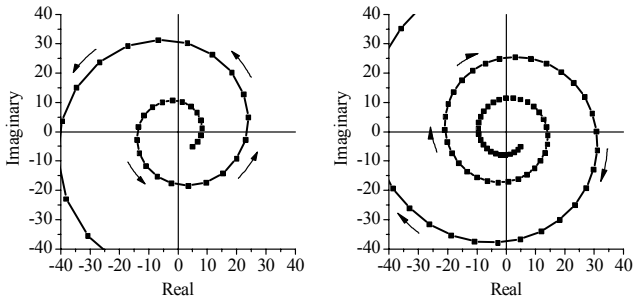

(a) below critical speed (34740 min^{-1})

(b) beyond critical speed (37200 min^{-1})

Fig.7 Polar plots of thermally induced vibration

beyond the critical speed.

V. Measurement of Thermally Induced Vibration

A. How to Pass the Critical Speed

It is difficult to measure the net residual unbalance for the first bending mode, because the vibration vector is subject to variation as time elapses in the situation that thermal bending occurs. UFRC is effective to restrain thermal bending and identify the unbalance [2]. The UFRC to the first bending mode can be achieved by setting $k_{nps} = 0$ in (2). By bringing the rotational speed close to the critical speed under UFRC operation, the net unbalance can be measured.

After balancing under UFRC operation, k_{nps} is reset back to the normal value (N-ps control) to pass the critical speed. Now, thermally induced vibration will increase and exceed the maximum allowable amplitude, if the rotational speed stays around the critical speed for long time. Hence, the change rate of the rotation speed must be increased as much as possible for passing the critical speed before the thermal bending occurs[2]. Fig. 8 is the unbalance response curve when the rotational speed actually passed the first bending critical speed. The influence from thermal bending can be reduced by bringing the rotational speed close to the first bending critical speed as much as possible under applying UFRC, and applying N-ps control only to a narrow range of the rotational speed including the first bending critical speed (34080 min^{-1} to 38880 min^{-1}). The actual acceleration rate of the inverter is set to 720 min^{-1}/sec.

B. Measurement Results of Thermally Induced Vibration

When the rotational speed was fixed at 34740 min^{-1}, which is slightly lower than the first bending critical speed, 36100 min^{-1} (actually measured value), unbalance vibration increased in a spiral manner as showing in Fig. 9(a). The rotational direction of the spiral is the same as that of the rotor. The dashed curve in the figure is the locus from 6000 min^{-1} to 34740 min^{-1}. This indicates that UFRC was applied from a rotational speed of 18000 min^{-1}, and N-ps control was additionally applied to the parallel system from 34200 min^{-1}. By aborting the N-ps control at 34740 min^{-1} and simply applying UFRC, this increase of vibration was stopped. This means that the cause of the vibration increase is the thermal deformation of the rotating part of the bearings due to the aforesaid iron loss.

Fig. 9(b) shows the variation in rotor displacement when the rotational speed is fixed at 34380 min^{-1}, which is slightly lower than that applied in Fig. 9(a). The displacement vector varies in the rotational direction of the rotor. However, it converges to a point without increasing. Figs. 9(a) and 9(b) indicate that there is a boundary of stability between 34380 min^{-1} and 34740 min^{-1}. Fig. 9(c) indicates the case in which the rotational speed exceeding the first bending critical speed is fixed at 37200 min^{-1}. The displacement vector increases spirally, but the direction of the spiral is opposite from the rotational direction of the

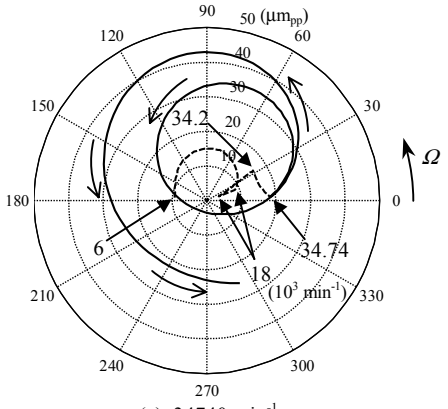

(a) 34740 min^{-1}

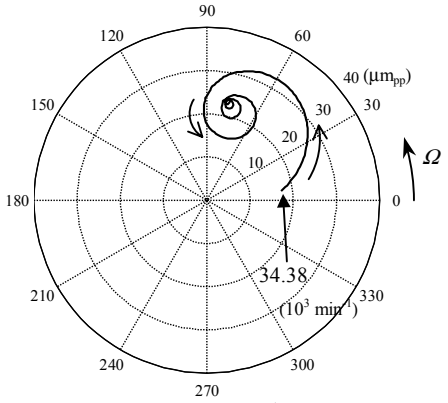

(b) 34380 min^{-1}

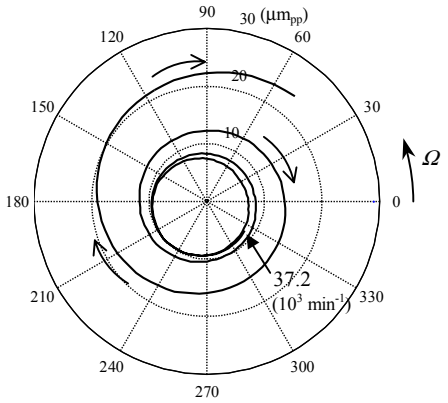

(c) 37200 min^{-1}

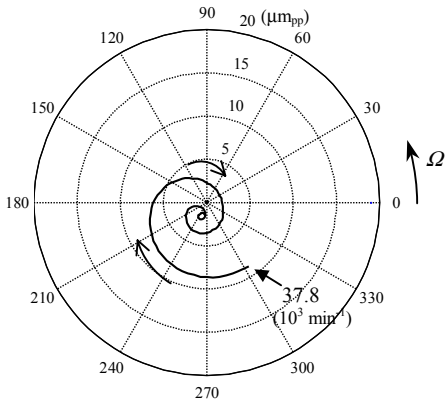

(d) 37800 min^{-1}

Fig.9 Polar plot of a measured spiral vibration at several rotational speeds (at y_2 axis)

rotor. This is the opposite result from the case in which the rotation speed is lower than the critical speed, and it supports the calculation results presented in the previous chapter. Fig. 9(d) indicates the case in which the rotational speed is fixed at 37800 min^{-1}, which is slightly higher than the above speed. Also in this case, the displacement vector draws a spiral in the opposite direction from the rotor rotation, but it converges to a point without increasing. Figs. (c) and (d) indicate that there is a boundary of stability between 37200 min^{-1} and 37800 min^{-1}. All the four measurement results mentioned above were within several minutes. It was confirmed from these results that instability is more significant as the rotation speed becomes closer to the critical speed, and the direction of the variation of rotor displacement differs depending on whether the rotational speed is lower than the critical speed or not.

C. Measurement of Instability of Thermally Induced Vibration

In this section, the measurement of $|H/P|$, which is a parameter influencing the stability of thermally induced vibration is presented. First of all, in order to avoid increasing vibration, disconnect the feedback loop by using UFRC. This means applying k_{nps} =0 to (5), which is equivalent to applying $C(j\Omega)$=0 to Fig. 6. Next, as shown in Fig. 6, generate a bearing force by a forward open loop excitation signal $Ae^{j(\Omega t+\phi)}$, and measure the rotor displacement caused by it. If things occur as shown in the model, a response by P should appear on the rotor displacement at the moment an excitation signal is applied, and a response by H should appear as time elapses.

Fig. 10 is a polar plot of the variation in the rotor displacement when an open loop excitation was actually applied at a rotational speed of 34200 min^{-1}, which is lower than the first bending critical speed. Fig. 11 indicates a plot of the variation of amplitude at that time on the horizontal axis of time. In these figures, the variation from (A) to (B) corresponds to the moment at which the open loop excitation was started, indicating the characteristic of P. The variation from (B) to (C) indicates the expression of the characteristic of H, showing that unbalance altered by the thermal bending induced by the excitation force. This is a slow change over several minutes. The variation from (A) to (B) is opposite to that from (B) to (C), and this indicates that the signs of P and H are opposite to each other. This corresponds to the relation of signs between (8) and (9) when rotational speed Ω is $\omega_2<\Omega<\omega_n$.

In this figure, length S_1 corresponds to $|P|$, and length S_2 corresponds to $|H|$. Consequently, the derived $|H/P|$ at a rotational speed of 34200 min^{-1} is approximately 2.0 based on Figs. 10 and 11. The time constant of thermal deformation, τ, is also determined as approximately 28 sec based on Fig. 11. These experimental results verify the expected behaviors from the model, and this supports the concept of the model.

Fig. 12 is a chart plotting $|H/P|$ measured at several rotational speeds. The solid line is the curve of the stability condition calculated based on (10). As shown in Fig. 9, there are boundaries of stability between 34380 min^{-1} and 34740 min^{-1}, and between 37200 min^{-1} and 37800 min^{-1}. The stable/unstable boundaries (frequencies)

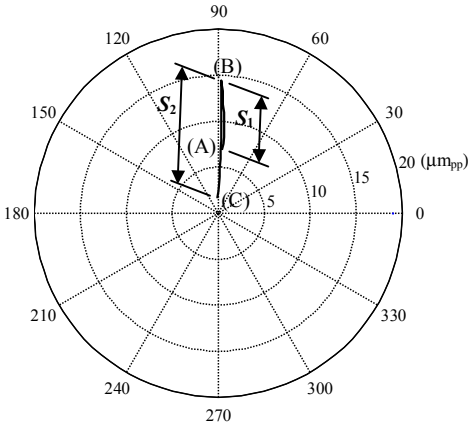

Fig.10 Position vector trajectory during an open loop excitation

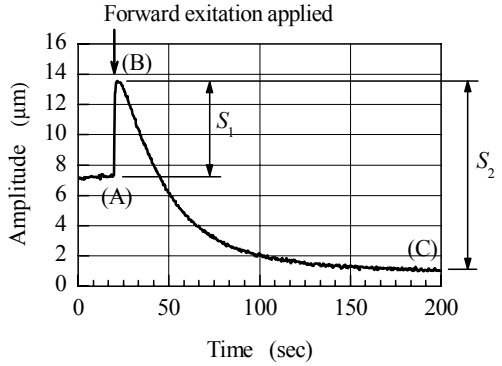

Fig.11 Time response during an open loop excitation

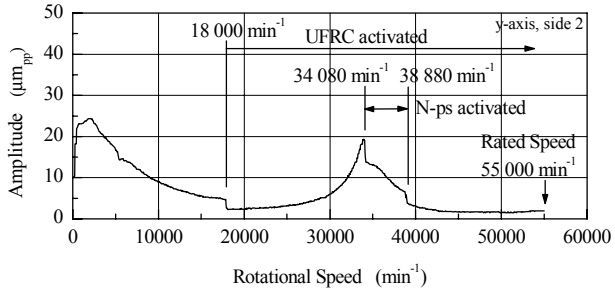

Fig.8 Unbalance response (at y_2 axis)

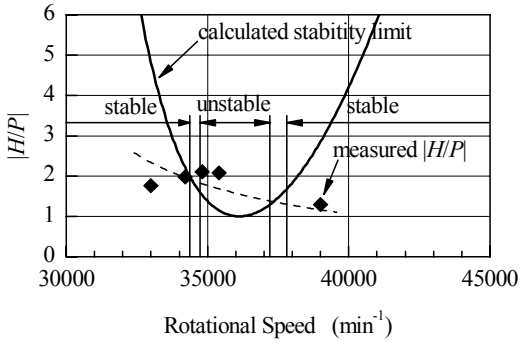

Fig.12 Stability chart of thermally induced vibration

expected from intersecting points between the measured $|H/P|$ plots and the curve of the stability condition (solid line) in Fig. 12 fit the results of Fig. 9 almost perfectly. The $|H/P|$ can be determined by calculation from (8) and (9) as follows,

$$\frac{H}{P} = \frac{H_0}{P_0(\omega_z{}^2 - \Omega^2)}. \tag{12}$$

The dashed curve on Fig. 12 indicates the calculated $|H/P|$ assuming as $|H/P|$=1.55 at $\Omega = \omega_n$. Although it is meaningless to compare absolute values due to using an assumed value in (12), it is meaningful to evaluate trends. The trend of the calculated curve does not match those of the measured plots at lower rotational speeds. However, they do match at higher rotational speeds.

VI. Conclusion

We reported the symptom of thermally induced vibration (increase of vibration in a spiral manner) caused by a biased distribution of iron loss on a high-speed turbo compressor of the AMB type.

To pass the critical speed with suppressing thermally induced vibration, it is effective to identify the balance by using UFRC and minimize the period of time in the unstable area by rapid acceleration and deceleration.

This time, we were able to pass the critical speed, and clarified experimentally that the spiral direction of vibration increase switches depending on whether the rotational speed is below or beyond the critical speed.

We formulated a method to measure $|H/P|$, which is a parameter to determine the instability of thermal bending. In the future, it will be important to be able to predict this parameter.

References

[1] S. Ishida, A. Maemura, T. Takakura, "Active Magnetic Bearing", *Yaskawa Technical Review*, vol. 57, no. 3, 1993, pp. 205-210.

[2] N. Takahashi, N. M. Hiroshima, H. Miura, Y. Fukushima, "Instability Induced by Iron Losses in Rotor-Active Magnetic Bearing System", in *Proc. 2nd International Symposium on Stability Control of Rotating Machinery*(*ISCORMA-2*), Gdańsk, 2003, pp. 627-636.

[3] J. Schmied, "Spiral Vibrations of Rotors", in *Proc. 11th Biennial ASME Vibration and Noise Conf.*, Boston, 1987, pp. 449-456.

[4] R. Liebich, T. Gach, "Spiral Vibration – Modal Treatment of a Rotor-rub Problem Based on Coupled Structural/Thermal Equations", *ImechE*, C500/42, 1996, pp. 205-210.

[5] R. G. Kirk, A. C. Balbahadur, "Thermal Distortion Synchronous Rotor Instability", *ImechE*, C576/41, 2000, pp. 427-436

[6] N. Takahashi, H. Miura, Y. Fukushima, "Design and Test Results of Active Magnetic Bearing Control System for High-speed Turbo Compressor", in *Proc. 9th MOVIC* Japan, pp. 48-53, Aug. 2005

[7] R. Gasch, H. Pfützner, *Rotordynamik - Eine Einführung*, Springer-Verlag, Berlin, Heidelberg, New York, 1975.